

Supplementary material for: “*The avalanche-like behaviour of large-scale hemodynamic activity from wakefulness to deep sleep*”

## 1. Model comparison

We compared the power-law fits performed in the main manuscript to three other distributions: log-normal, power-law with exponential cutoff, and truncated power-law (at cluster size  $10^3$ ) (following Clauset et al., 2009). In the following, all empirical distributions are understood to be the cluster size distributions. The first two distributions have an additional parameter compared to a standard power-law and reduce to it within a range of parameter values. Therefore, it is expected that the goodness-of-fit (GoF) obtained using these models is similar or better than that obtained using the unmodified power-law, and that the presence of power-law behavior can be decided based on whether the estimated parameters are within the above-mentioned range of values.

The details of the three models are the following:

1. Log-normal distribution, given by  $P(x; \mu, \sigma) = \frac{1}{\sigma\sqrt{2\pi}} \exp\left[-\frac{(\ln x - \mu)^2}{2\sigma^2}\right]$ . This distribution has one additional free parameter to adjust vs. the power-law distribution. However, in the limit of large  $\sigma$ , it can be shown that  $P(x; \mu, \sigma)$  behaves as a power-law with an exponent given by  $-\frac{\mu}{\sigma^2} + 1$  (see the approximation in Mitzenmacher, 2004).
2. Power-law with exponential cutoff, given by  $P(x; \alpha, \beta) \propto x^{-\alpha} \exp(-\beta x)$ . Again, we note that this distribution has one additional free parameter to adjust compared to a standard power-law distribution; however, for  $\beta \approx 0$ , its behavior approximates that of a power-law. See Klaus et al. (2011) for an application of this distribution to the characterization of neuronal avalanches.
3. Truncated power-law distribution, i.e. a power-law not only limited in its lower range by  $x_{\min}$ , but also limited in its upper range by  $x_{\max}$ , thus effectively avoiding the tail of the distribution.

### *Log-normal distribution*

The left panel of **Fig. S1** presents the log-likelihood ratios (llr) of the power-law (PL) vs. the log-normal (LN) distribution. The values of the log-likelihood ratios are balanced in sign, indicating comparable evidence favoring both models. The right panel of **Fig. S1** presents the p-values for rejecting the null hypothesis of equal distributions (obtained from Vuong’s test [Genius and Strazzer, 2002]). Clearly, rejecting the null hypothesis is not warranted by the resulting p-values. This is consistent with the estimated  $\sigma$  parameters which are, on average,  $\sim 40$ . In this limit where the log-normal presents power-law behavior, the combination of parameters  $-\frac{\mu}{\sigma^2} + 1$  should closely match the  $\alpha$  estimated using a standard power-law. This is shown in **Fig. S2** which presents,

side-by-side, the scaling exponents  $\alpha$  as inferred from fitting the data using a power-law (left) and a log-normal distribution, taking  $\alpha = -\frac{\mu}{\sigma^2} + 1$  (right).

Finally, in **Fig. S3** we show that the GoF obtained using power-law and log-normal distributions presents similar qualitative behavior across wakefulness and all sleep stages; in particular, the GoF is worst for N2 sleep. Here, the GoF are given by the Kolmogorov-Smirnov distances ( $D_{KS}$ ) between the empirical and fitted distributions; thus, higher  $D_{KS}$  implies a worse fit and vice-versa.

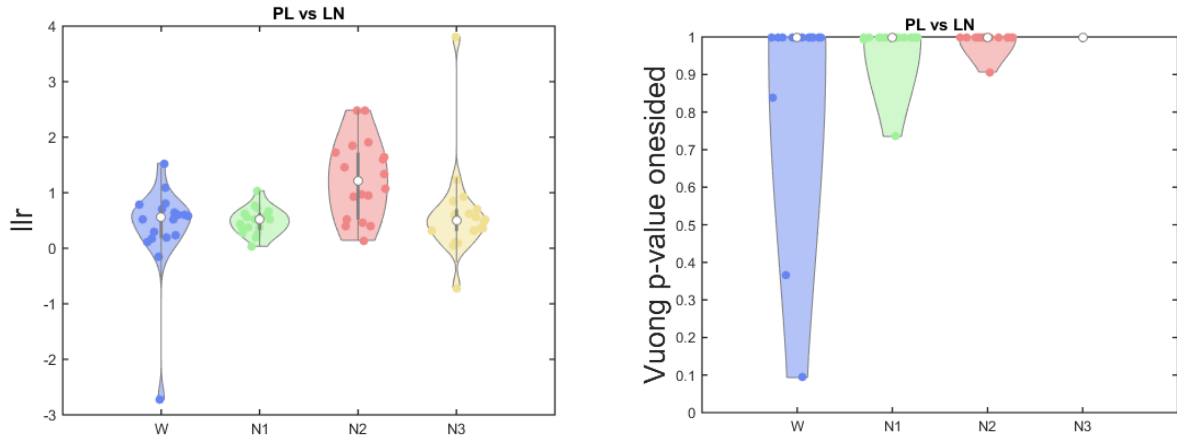


**Figure S1.** The log-likelihood ratio (llr) for power-law vs. log-normal (left), and the p-value for rejecting the null hypothesis of equal distributions (right).

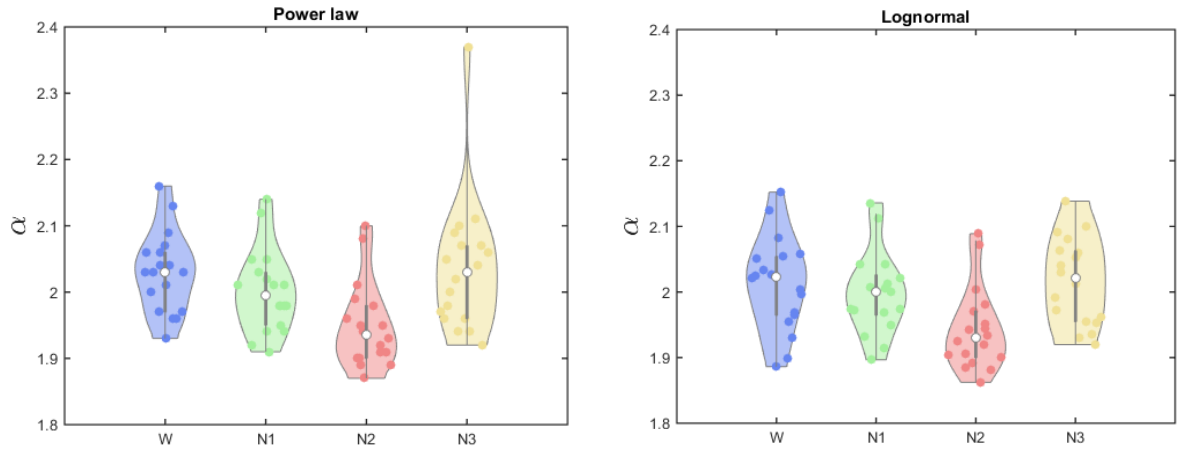


**Figure S2.** The scaling parameters  $\alpha$ , estimated from fitting the data using power-laws (left), and using log-normal distributions (right). The similarity between both sets of optimal values is evident. For the log-normal, the results of statistical tests are the following:  $p_{KW} = 0.0042$  (Kruskal-Wallis test for the effect of sleep stage on  $\alpha$ );  $p_{WvsN1} = 0.43$ ,  $p_{WvsN2} = 0.0051$ ;  $p_{WvsN3} = 0.83$  (post-hoc Wilcoxon tests for the differences between wakefulness, N1, N2 and N3, respectively).

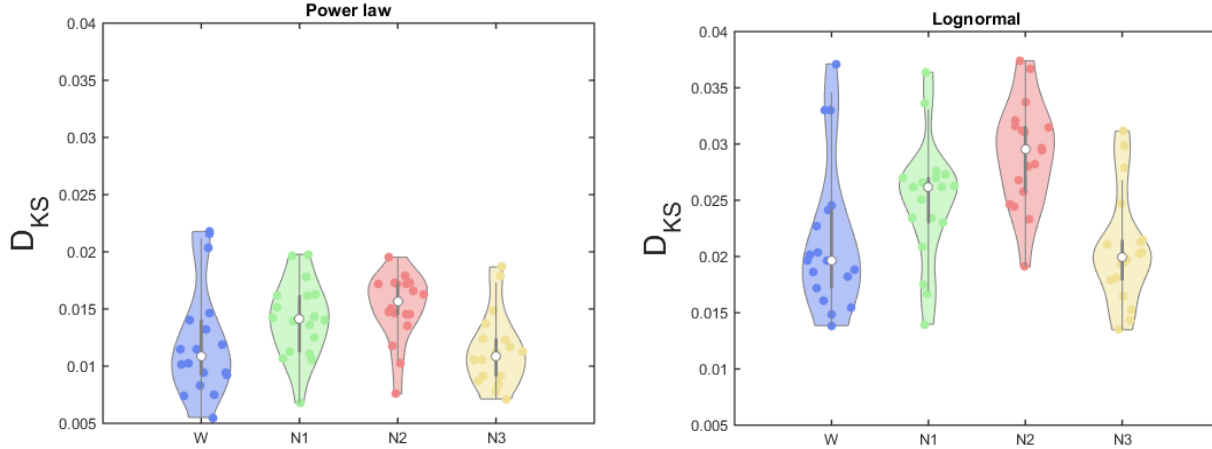


**Figure S3.** Kolmogorov-Smirnov distances ( $D_{KS}$ ) between the empirical distributions for cluster sizes and the fitted statistical models. Results are shown for standard power-laws (left), and log-normal distributions (right). Both sets of values are very similar, and in both N2 sleep presents the worst fit (i.e. the highest  $D_{KS}$ ).

#### *Power-law with exponential cutoff*

Analogous results were obtained fitting the empirical distributions using power-laws with exponential cutoffs. In this case, the small negative log-likelihood ratios indicate marginally better GoF for power-laws with exponential cutoff (**Fig. S4**, left), however, the p-values indicate that the rejection of the null hypothesis of equal distributions is not warranted (**Fig. S4**, right).

The estimated  $\beta$  parameters, representing the degree of exponential decay, are in all cases very close to zero (see **Fig. S5**). This suggests that the power-laws with exponential cutoff, when fitted to the empirical distributions, will present power-law behavior, with the estimated scaling exponents closely matching those obtained fitting unmodified power-laws. This is indeed the case, as shown in **Fig. S6**.

Finally, as in the case of the log-normal distribution, the GoF also achieved its worst value for N2 sleep (see **Fig. S7**).

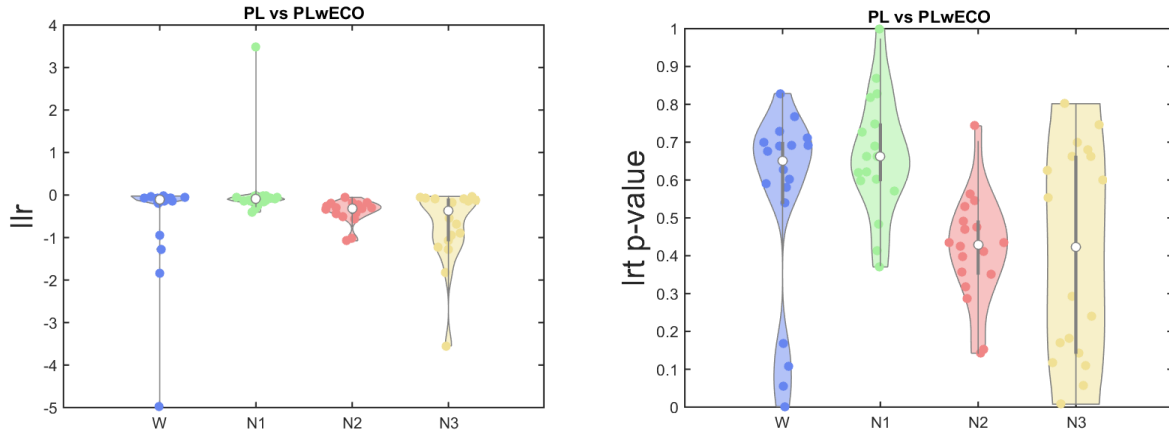


**Figure S4.** The log-likelihood ratio (llr) for power-law vs. power-law with exponential cutoff (left), and the p-value for rejecting the null hypothesis of equal distributions (right).

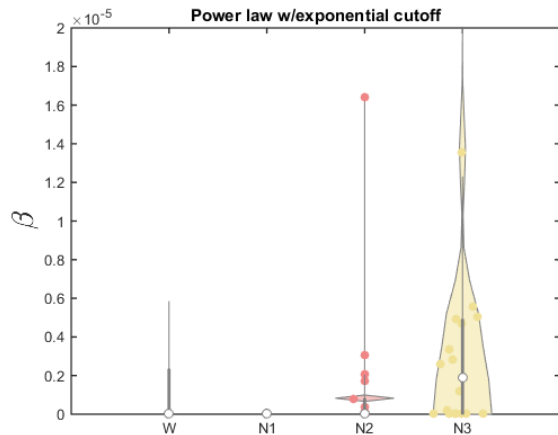


**Figure S5.** Estimated parameters for the exponential cutoffs  $\beta$ . The negligible effect of the exponential cutoff is evident from observing that, for almost all subjects and stages,  $\beta < 10^{-5}$ .

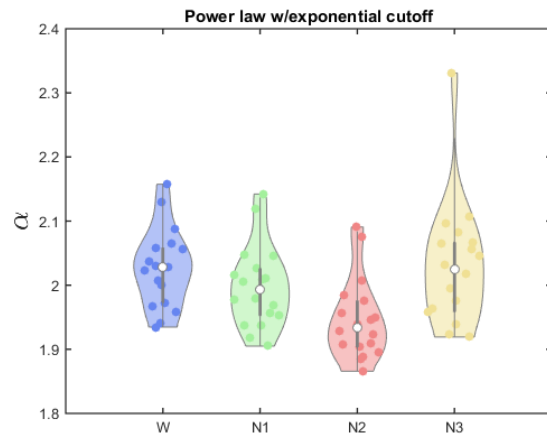
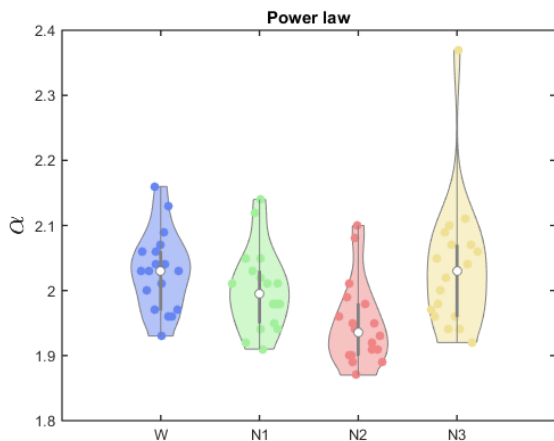


**Figure S6.** The scaling parameters  $\alpha$ , estimated from fitting the data using power-laws (left), and using power-laws with exponential cutoff (right). The similarity between both sets of optimal values is evident. For the power-law with exponential cutoff, the results of statistical tests are the following:  $p_{KW} = 0.0013$  (Kruskal-Wallis test for the effect of sleep stage on  $\alpha$ );  $p_{WvsN1} = 0.11$ ,  $p_{WvsN2} = 0.0007$ ,  $p_{WvsN3} = 0.91$  (post-hoc Wilcoxon tests for the differences between wakefulness, N1, N2 and N3, respectively).

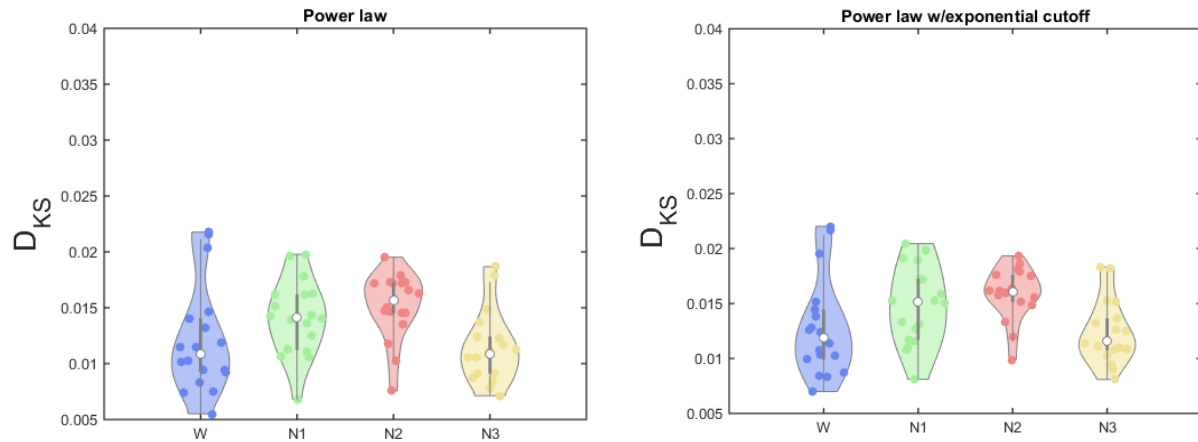


**Figure S7.** Kolmogorov-Smirnov distances ( $D_{KS}$ ) between the empirical distributions for cluster sizes and the fitted statistical models. Results are shown for standard power-laws (left), and power-laws with exponential cutoff (right). Both sets of values are very similar, and in both N2 sleep presents the worst fit (i.e. the highest  $D_{KS}$ ).

### *Truncated power laws*

Finally, we show that the scaling parameters  $\alpha$  can be obtained fitting the data using power-law distributions for cluster sizes truncated at  $10^3$  (**Fig. S8**). Thus, the scaling parameters  $\alpha$  do not differ solely due to the events located at the tail of the distributions. In addition, the GoF obtained using the truncated distributions (in terms of  $D_{KS}$ ) is the worst for N2 sleep, consistent with the results obtained using other distributions (**Fig. S9**).

These results, together with those obtained from fitting power-laws with exponential cutoffs and log-normals, provide evidence supporting that our conclusions do not arise as a consequence of finite size effects manifesting at the tail of the distributions.

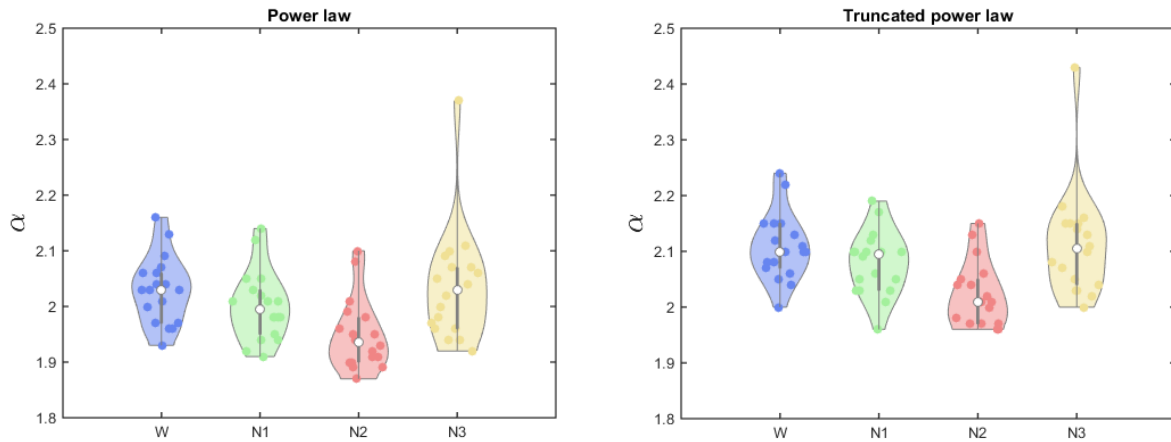


**Figure S8.** The scaling parameters obtained from power-law distributions for cluster sizes truncated at  $10^3$ . The results of statistical tests are the following:  $p_{KW} = 6.2e-04$  (Kruskal-Wallis test for the effect of sleep stage on  $\alpha$ );  $p_{WvsN1} = 0.16$ ,  $p_{WvsN2} = 0.0003$ ;  $p_{WvsN3} = 0.86$  (post-hoc Wilcoxon tests for the differences between wakefulness, N1, N2 and N3, respectively).

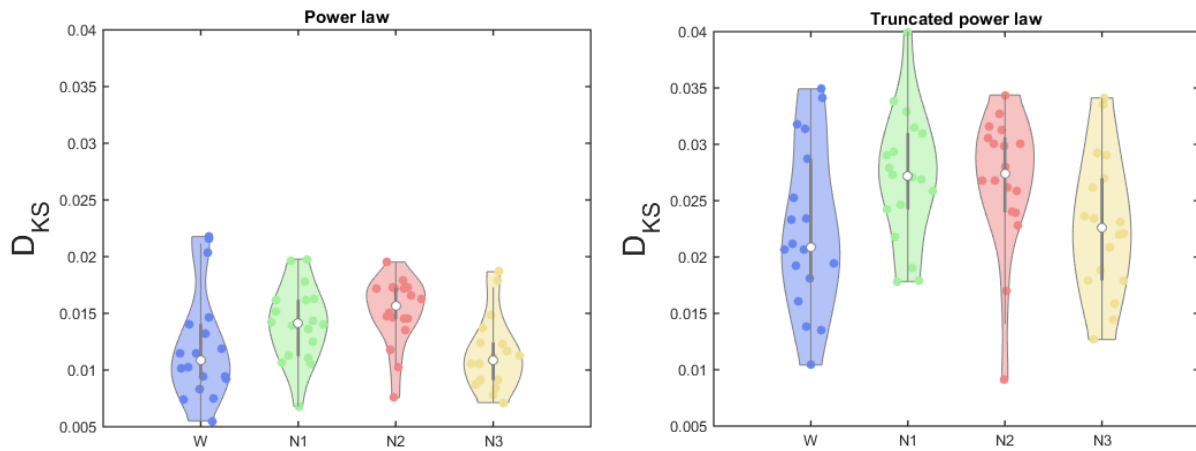


**Figure S9.** Kolmogorov-Smirnov distances ( $D_{KS}$ ) between the empirical distributions for cluster sizes and the fitted statistical models. Results are shown for standard power-laws (left), and truncated power-laws (right). Both sets of values are very similar, and in both N2 sleep presents the worst fit (i.e. the highest  $D_{KS}$ ).

## 2. Individual complementary cumulative distribution functions (CCDF) fitted with power-laws

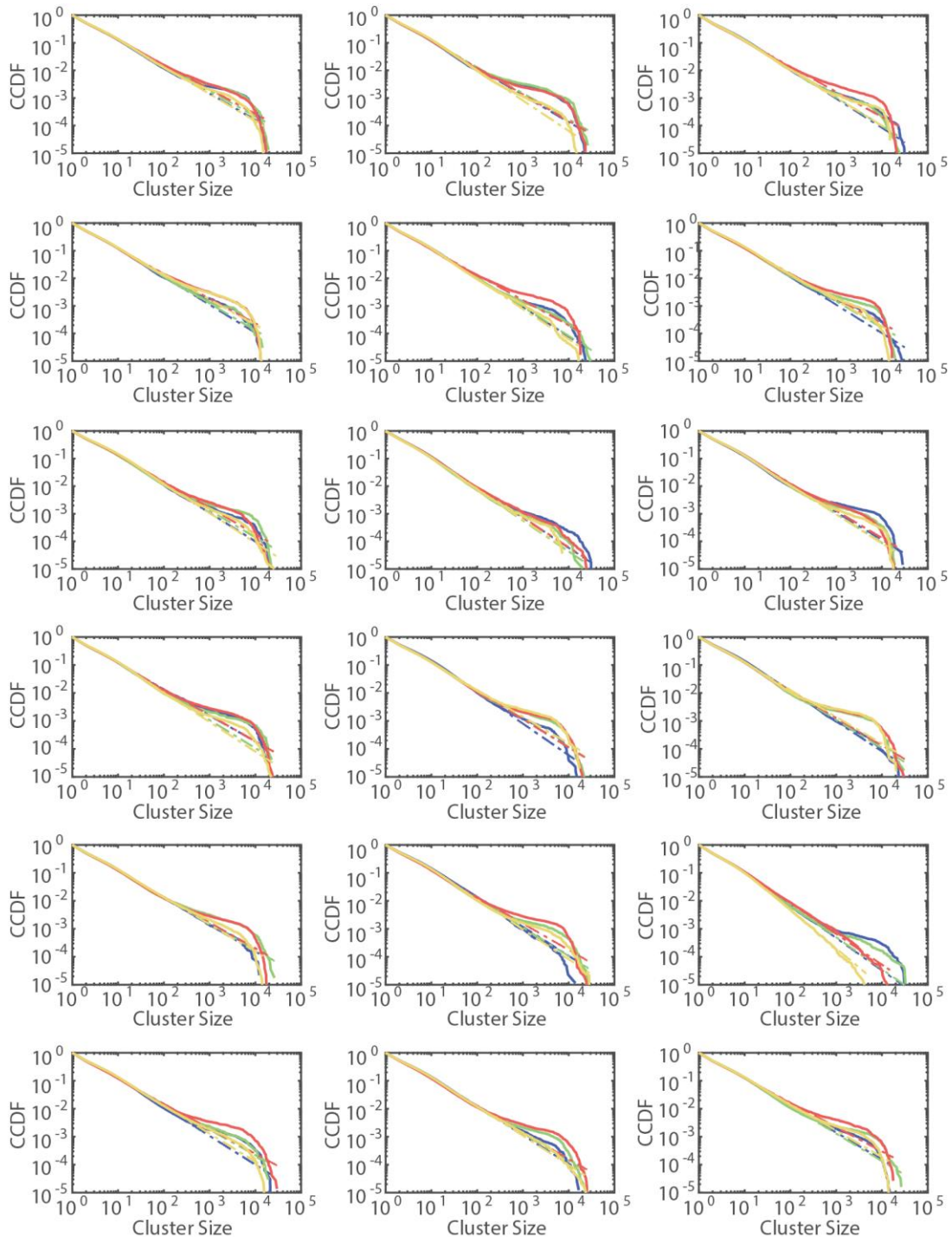


**Figure S10.** Complementary cumulative distribution functions (CCDF) for cluster sizes of each individual participant. Different colors indicate wakefulness, N1, N2 and N3 (same code as in the manuscript figures). The dashed lines indicate the best fitting power-law distributions.

### 3. Individual complementary cumulative distribution functions (CCDF) fitted with truncated power-laws

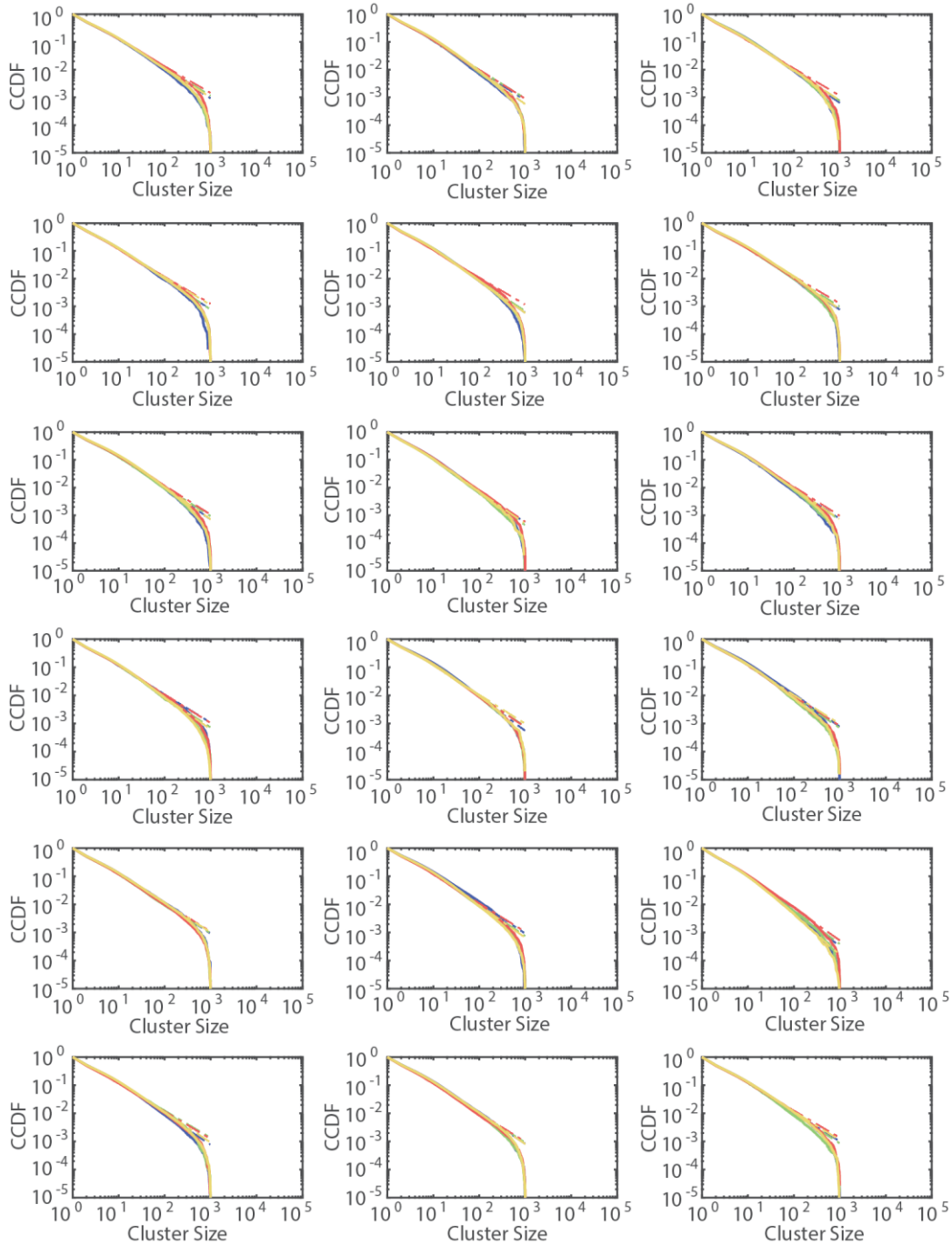


**Figure S11.** Complementary cumulative distribution functions (CCDF) for cluster sizes of each individual participant. Distributions appear truncated at  $10^3$ . Different colors indicate wakefulness, N1, N2 and N3 (same code as in the manuscript figures). The dashed lines indicate the best fitting truncated power-law distributions.

4. Individual complementary cumulative distribution functions (CCDF) fitted with power-laws with exponential cutoff

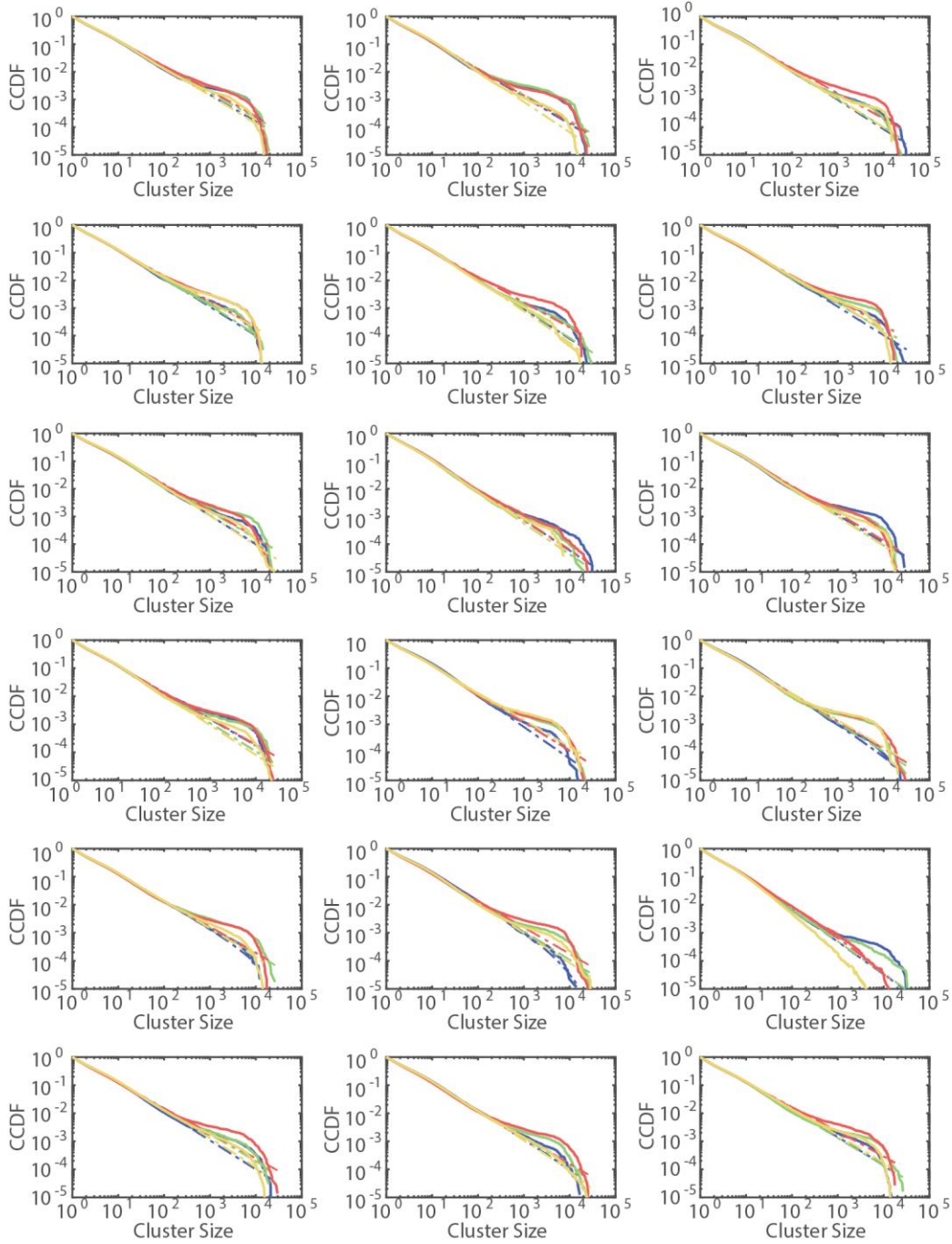


**Figure S12.** Complementary cumulative distribution functions (CCDF) for cluster sizes of each individual participant. Different colors indicate wakefulness, N1, N2 and N3 (same code as in the manuscript figures). The dashed lines indicate the best fitting power-laws with exponential cutoff.

## 5. Prevalence of the different sleep stages in the dataset

We investigated the possibility that our results are influenced by different levels of sampling in the dataset, both in terms of the total number of included fMRI volumes and connected clusters of voxels included in the computation of the cluster size distributions. As shown in **Fig. S13**, neither quantity presents a singularity for N2 sleep. Both in terms of volumes and total number of clusters considered in the analysis, N2 sleep is sampled at a degree comparable to that of wakefulness. N1 sleep is the most underrepresented stage in our dataset. As expected, there exists a positive correlation between the total number of volumes and cluster sizes considered (shown in the rightmost panel of **Fig. S13**).

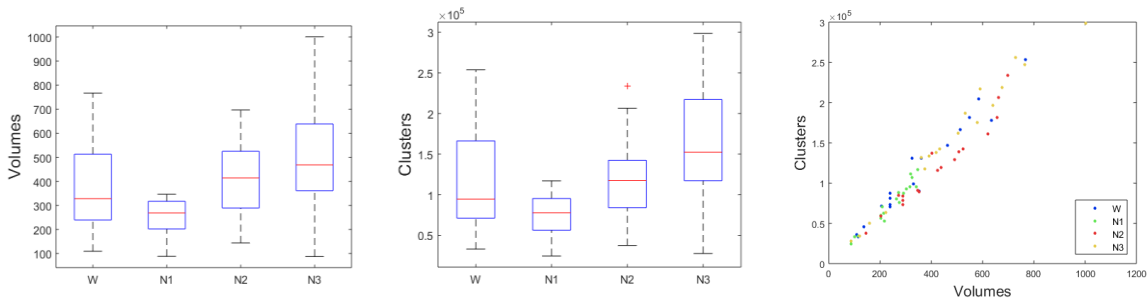


**Figure S13.** Statistics concerning the level of sampling of the different sleep stages. Right: total number of volumes considered per sleep stage. Center: total number of connected clusters of voxels considered per sleep stage. Right: scatter plot showing the positive correlation between volumes and clusters (each point corresponds to an individual participant, and the sleep stage is indicated using the color code detailed in the inset).  $P_{KS} = 0.0019$  (Kruskal-Wallis test for the number of volumes vs. sleep stage),  $p_{WvsN1} = 0.07$ ,  $p_{WvsN2} = 0.22$ ,  $p_{WvsN3} = 0.11$  (post-hoc Wilcoxon tests for the number of volumes in wakefulness vs. N1, N2 and N3 sleep).  $P_{KS} = 0.0039$  (Kruskal-Wallis test for the number of clusters vs. sleep stage),  $p_{WvsN1} = 0.06$ ,  $p_{WvsN2} = 0.66$ ,  $p_{WvsN3} = 0.12$  (post-hoc Wilcoxon tests for the number of clusters in wakefulness vs. N1, N2 and N3 sleep). Spearman's rank correlation coefficient for the number volumes vs number of clusters  $\rho = 0.9809$ ,  $p = 1.5e-51$ .

To assess whether the level of sampling biased the estimated scaling parameters, we investigated their correlation using the non-parametric Spearman's rank correlation. Scatter plots of the estimated  $\alpha$  vs. the number of fMRI volumes and analyzed connected clusters per sleep stage are shown in **Fig. S14**. The results do not indicate a significant association between the variables.

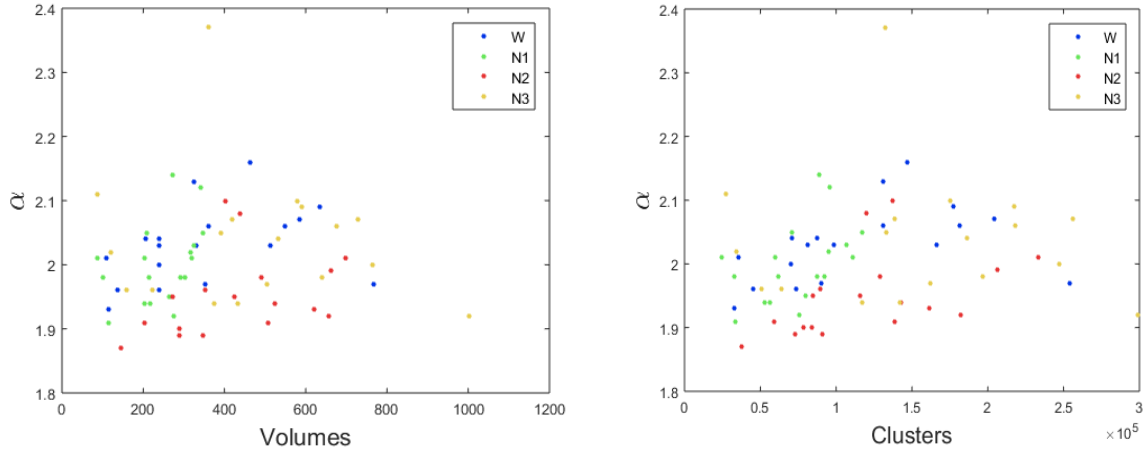


**Figure S14.** Scatter plots of the scaling exponent  $\alpha$  vs. the number of volumes and clusters of connected voxels for each sleep stage (each point corresponds to an individual participant, and the sleep stage is indicated using the color code detailed in the inset). Spearman's rank correlation coefficient for  $\alpha$  vs number of volumes  $\rho=0.19$ ,  $p=0.09$ . Spearman's rank correlation coefficient for  $\alpha$  vs number of volumes  $\rho=0.30$ ,  $p=0.01$ .

Completely analogous results were obtained for truncated power laws, as shown in **Fig. S15**

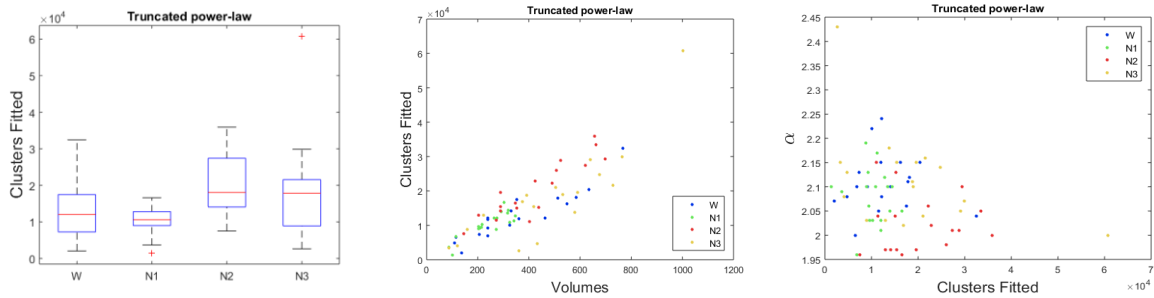


**Figure S15.** The scaling parameters do not depend on the number of clusters of connected voxels when fitted using a truncated power-law. Left: number of clusters considered when fitting with truncated power-laws. Center: number of clusters vs. number of volumes per sleep stage when fitting with truncated power-laws. Right: the scaling exponent  $\alpha$  vs. the number of clusters fitted using truncated power-laws (each point corresponds to an individual participant, and the sleep stage is indicated using the color code detailed in the inset).  $p_{KS} = 0.0013$  (Kruskal-Wallis test for the number of clusters vs. sleep stage),  $p_{WvsN1} = 0.30$ ,  $p_{WvsN2} = 0.01$ ,  $p_{WvsN3} = 0.15$  (post-hoc Wilcoxon tests for the number of clusters in wakefulness vs. N1, N2 and N3 sleep). Spearman's rank correlation coefficient for number of clusters vs. number of volumes  $\rho=0.84$ ,  $p=1.03e-20$ . Spearman's rank correlation coefficient for  $\alpha$  vs number of clusters  $\rho=-0.20$ ,  $p=0.08$ .

## 6. Statistics of cluster size distributions obtained using shuffled time series

In **Fig. 4** of the main manuscript text we present the CCDF obtained after phase shuffling the time series of each individual voxel. The cluster size distributions obtained from statistically independent point-processes are predicted to follow Poisson distributions; however, we note that in order to provide a fairer null model, we did not shuffle the point-processes, but the phases of the BOLD signals which (after thresholding) yielded in the point-process. As shown by Touboul and Destexhe (2010), thresholded statistically independent continuous stochastic processes present distributions of super-threshold events deviating from the Poisson distribution. Following Touboul and Destexhe, we fitted a power-law with exponential cutoff and then investigated whether the cutoff parameter fulfilled  $\beta \gg 0$ , indicating a significant exponential decay.

**Fig. S16** presents the empirical distribution, together with the optimal Poisson and power-law with exponential cutoff distributions fitted to the data. It is clear from visual inspection that, as expected, the Poisson distribution presents a suboptimal fit, and that a relatively good fit was obtained for the power-law with exponential cutoff. The estimated exponential cutoff parameter is  $\beta=0.15$ . This value is on average nine orders of magnitude ( $> 10^9$ ) larger than the  $\beta$  values obtained based on the unshuffled time series (see **Fig. S5**). Thus, the power-law obtained from the shuffled data is heavily modulated by exponential decay.

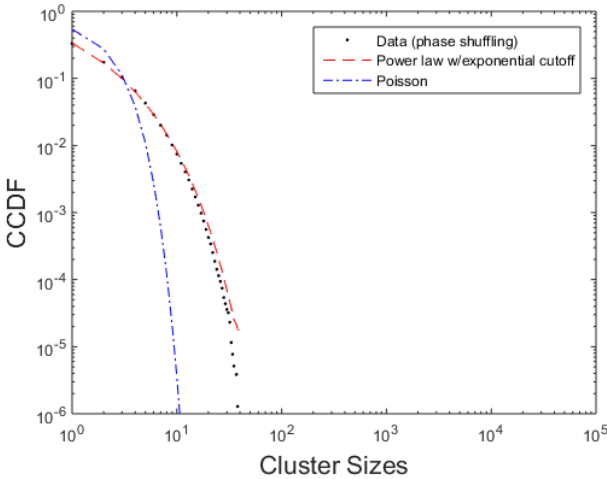


**Figure S16.** The empirical CCDF for the distribution of clusters sizes, together with the best fit using Poisson and power-law with exponential cutoff distributions.

## 7. Two-point spatial correlation functions

As an independent marker of scale-free behavior in the data, we investigated the scaling of the two-point correlation functions, as defined in Expert et al. (2010). We computed the correlation matrix between all pairs of voxels within grey matter (i.e. those voxels belonging to at least one region in the Automated Anatomic Labeling atlas [Tzourio-Mazoyer et al., 2002]),  $C_{ij} = \rho(x_i(t), x_j(t))$ , where  $\rho(x, y)$  represents Pearson's linear correlation coefficient between signals  $x$  and  $y$ , and  $x_i(t)$  represents the fMRI BOLD time series at the  $i$ -th voxel. We also computed the matrix of Euclidean distances between all pairs of voxels,  $D_{ij}$ . From these two matrices, the two-point correlation function  $\langle C(r) \rangle$  was computed as the mean of all  $C_{ij}$  entries fulfilling that  $r \leq D_{ij} \leq r + r_0$ , where  $r_0$  is the minimum possible Euclidean distance between voxels at the current resolution (4 mm).

The shape of the resulting  $\langle C(r) \rangle$  for all sleep stages (in log-log scale) is shown in **Fig. S17**. The shape of the distributions (including the slope of the linear regime) very closely resembles those presented in **Fig. 1B** of Expert et al. (2010). Consistently with the results published by Expert and colleagues, the correlation function decreases for a range of  $r$  but then presents a plateau and, afterwards, rises again to reach values comparable to those at the left end of the distribution. This was identified by Expert and colleagues as a consequence of the correlation structure of typical resting state fMRI data; more precisely, as arising due to the abnormally high correlation coefficient between homotopic voxels (i.e. those voxels that are symmetric with respect to the left-right divide) (Salvador et al., 2005a; Salvador et al., 2005b).

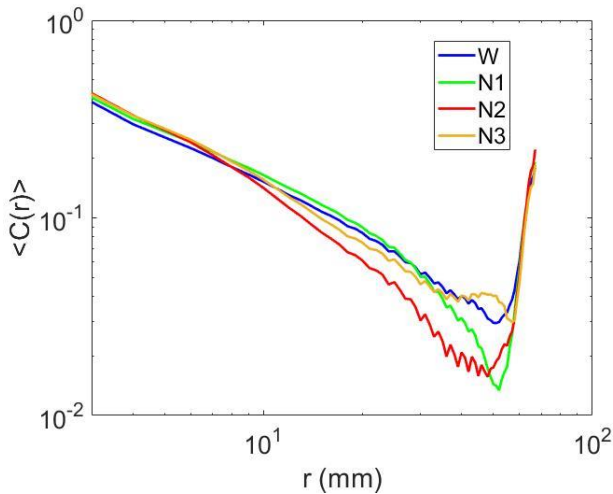


**Figure S17.** The correlation function  $\langle C(r) \rangle$  for wakefulness and all stages of NREM sleep.  $\langle C(r) \rangle$  was computed following Expert et al. (2010).

## References

- Clauset, A., Shalizi, C. R., & Newman, M. E. (2009). Power-law distributions in empirical data. *SIAM review*, 51(4), 661-703.
- Expert, P., Lambiotte, R., Chialvo, D. R., Christensen, K., Jensen, H. J., Sharp, D. J., & Turkheimer, F. (2010). Self-similar correlation function in brain resting-state functional magnetic resonance imaging. *Journal of The Royal Society Interface*, 8(57), 472-479.
- Genius, M., & Strazzer, E. (2002). A note about model selection and tests for non-nested contingent valuation models. *Economics Letters*, 74(3), 363-370.
- Klaus, A., Yu, S., & Plenz, D. (2011). Statistical analyses support power law distributions found in neuronal avalanches. *PloS one*, 6(5), e19779.
- Mitzenmacher, M. (2004). A brief history of generative models for power law and lognormal distributions. *Internet mathematics*, 1(2), 226-251.
- Salvador, R., Suckling, J., Schwarzbauer, C., & Bullmore, E. (2005a). Undirected graphs of frequency-dependent functional connectivity in whole brain networks. *Philosophical Transactions of the Royal Society B: Biological Sciences*, 360(1457), 937-946.
- Salvador, R., Suckling, J., Coleman, M. R., Pickard, J. D., Menon, D., & Bullmore, E. D. (2005b). Neurophysiological architecture of functional magnetic resonance images of human brain. *Cerebral cortex*, 15(9), 1332-1342.
- Touboul, J., & Destexhe, A. (2010). Can power-law scaling and neuronal avalanches arise from stochastic dynamics?. *PloS one*, 5(2), e8982.
- Tzourio-Mazoyer, N., Landeau, B., Papathanassiou, D., Crivello, F., Etard, O., Delcroix, N., et al. (2002). Automated anatomical labeling of activations in SPM using a macroscopic anatomical parcellation of the MNI MRI single-subject brain. *Neuroimage*, 15(1), 273-289.